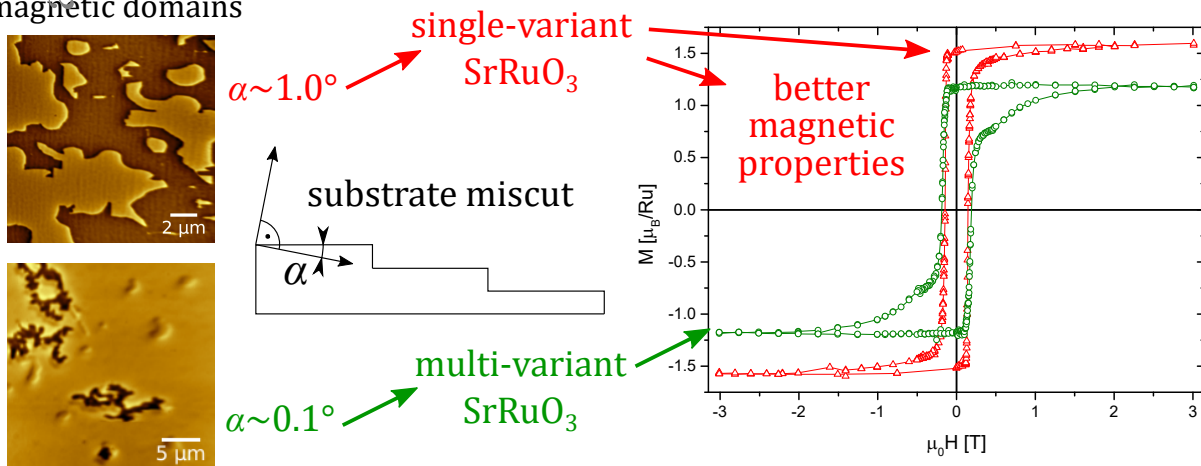


# Graphical Abstract

## Magnetic domain wall motion in SrRuO<sub>3</sub> thin films

Martin Zahradník, Klára Uhlířová, Thomas Maroutian, Georg Kurij, Guillaume Agnus, Martin Veis, Philippe Lecoeur

magnetic domains



## Highlights

### **Magnetic domain wall motion in SrRuO<sub>3</sub> thin films**

Martin Zahradník, Klára Uhlířová, Thomas Maroutian, Georg Kurij, Guillaume Agnus, Martin Veis, Philippe Lecoeur

- Spatially resolved dynamics of SrRuO<sub>3</sub> magnetization was captured at low temperatures.
- Low-miscut angle ( $\sim 0.1^\circ$ ) of SrTiO<sub>3</sub> substrate leads to increased density of domain nucleation and pinning centers in SrRuO<sub>3</sub> films.
- Presence of anti-phase boundaries results in magnetic structures persisting up to high magnetic fields ( $\sim 14$  T).

# Magnetic domain wall motion in SrRuO<sub>3</sub> thin films

Martin Zahradník<sup>a,b,\*</sup>, Klára Uhlířová<sup>a</sup>, Thomas Maroutian<sup>b</sup>, Georg Kurij<sup>b</sup>, Guillaume Agnus<sup>b</sup>, Martin Veis<sup>a</sup> and Philippe Lecoeur<sup>b</sup>

<sup>a</sup>Charles University, Faculty of Mathematics and Physics, Ke Karlovu 3, 12116 Prague 2, Czech Republic

<sup>b</sup>Centre for Nanoscience and Nanotechnology (C2N), CNRS UMR 9001, Univ Paris-Sud, Université Paris-Saclay, 91120 Palaiseau, France

## ARTICLE INFO

### Keywords:

SrRuO<sub>3</sub>  
substrate miscut  
pulsed laser deposition  
magnetization relaxation

## ABSTRACT

Influence of substrate miscut on magnetization dynamics in SrRuO<sub>3</sub> (SRO) thin films was studied. Two films were grown on SrTiO<sub>3</sub> substrates with high ( $\sim 1^\circ$ ) and low ( $\sim 0.1^\circ$ ) miscut angles, respectively. As expected, high miscut angle leads to suppression of multi-variant growth. By means of SQUID magnetometry, comparable relaxation effects were observed in both the multi-variant and the nearly single-variant sample. Differences in the magnetization reversal process were revealed by magnetic force microscopy. It showed that the multi-variant growth leads to higher density of defects acting as pinning or nucleation sites for magnetic domains, which consequently results in deterioration of magnetic properties. It was demonstrated that the use of high miscut substrate is important for fabrication of high quality SRO thin films with low density of crystallographic defects and excellent magnetic properties.

## 1. Introduction

SrRuO<sub>3</sub> (SRO) is a well known itinerant ferromagnet ( $T_{C,bulk} \sim 160$  K [1]) that offers a broad range of applications in oxide electronics. Good conducting properties in combination with nearly ideal epitaxial growth have made it the most popular material for electrode fabrication in oxide heterostructures [2, 3]. In addition, multilayer systems of SRO and other oxide materials, such as SrTiO<sub>3</sub> (STO) [4] or La<sub>2/3</sub>Sr<sub>1/3</sub>MnO<sub>3</sub> (LSMO) [5, 6], exhibit suitable properties for fabrication of all-oxide magnetic tunnel junctions (MTJ).

One of the key functional elements of the MTJ is a stable pinning layer. To obtain a stable pinning layer, various approaches can be used. One of the promising ways is the use of LSMO/SRO bilayer, which exhibits antiferromagnetic coupling at the interface, although both individual materials are ferromagnetic. While this antiferromagnetic coupling has been thoroughly investigated [7, 8, 9, 10], its origin still remains unclear. To elucidate possible mechanisms laying behind this phenomenon, at first, detailed understanding of magnetic behaviour of SRO is essential.

Despite several decades of investigation, knowledge of the exact nature of magnetic anisotropy of SRO is still lacking in both bulk SRO [2] as well as in thin films [11]. Thin films of SRO exhibit ferromagnetic ordering below  $T_{C,film} \sim 150$  K [12] and unusual uniaxial magnetocrystalline anisotropy. Above  $T_C$  the easy axis of magnetization lies in the (001) orthorhombic plane and it is identical with the  $b$  orthorhombic axis, i.e. its direction is  $\sim 45^\circ$  inclined to the surface normal [13]. Below  $T_C$ , the easy axis remains in the (001) plane, however it rotates from the surface normal from  $\sim 45^\circ$  to  $\sim 30^\circ$  with decreasing temperature [14].

This peculiar temperature dependence of magnetocrystalline anisotropy is still subject of a scientific debate. Growth of SRO on the most commonly used STO substrate is possible in six different crystallographic orientations [15]. How-

ever, it has been found that the anisotropy is independent of the orientation [16]. Others attribute changes in the magnetocrystalline anisotropy to distortions of the SRO unit cell during the deposition process [17]. Kolesnik *et al.* [18] argue the effect of twinning, comparing the anisotropy in twinned and untwinned SRO films.

An additional important issue is arising as attempts of magnetization switching in SRO films are emerging. After current induced domain wall nucleation [19] and domain wall motion [20] was presented, temperature induced [21] as well as current induced [22, 23] magnetization reversal in SRO films was demonstrated. Another study reported on periodic control of magnetization via piezoelectric substrate in SRO/Pb(Mg<sub>1/3</sub>Nb<sub>2/3</sub>)O<sub>3</sub>-PbTiO<sub>3</sub> heterostructure [24]. All such attempts lead to possible applications in spintronic devices. For their proper functioning, not only a precise description of magnetic anisotropy, but also detailed knowledge of dynamic behaviour of magnetic domains is required.

Magnetic domain dynamics consists of two main mechanisms: domain nucleation, and domain wall motion (propagation). It has been already observed by Barkhausen in 1919, when he detected the so called Barkhausen noise, that the magnetization reversal process is not continuous [25]. It is due to the fact that both formation of domains, and domain wall motion needs activation energy to overcome a critical domain size, and to release the domain walls from pinning centers, respectively. Visualisation of the magnetization reversal can be realized not only by measuring Barkhausen noise, but also by direct techniques. Especially when the dynamics is slow enough, magnetic domains can be observed, e.g. by Kerr microscopy [26], or even magnetic force microscopy (MFM) [27].

This study reports on time evolution of magnetic domains in multi-variant and nearly single-variant SRO thin films. Superconducting quantum interference device (SQUID) magnetometry and magnetic force microscopy (MFM) was used to investigate the magnetization dynamics and mag-

\*Corresponding author

ORCID(s): 0000-0001-7660-5055 (M. Zahradník)

netic domain formation of both the multi-variant and the nearly single-variant SRO thin films. Pronounced differences in the magnetic domain wall motion behaviour were observed. It was argued that those differences originate in crystallographic defects induced by multi-variant growth of the films. Such findings are of high importance for design and realisation of all-oxide MTJ and new spintronic devices, because desired magnetic properties in SRO films could be tuned either by proper selection of substrate miscut angle, or even more generally by any parameters of the deposition process that directly influence crystallinity of the films.

Moreover, the present study demonstrates a pioneering aspect in investigation of SRO magnetic properties, which can be further generalised even for other material systems with low Curie temperature. Proper investigation of such materials ( $T_C < \text{room temperature}$ ) in terms of magnetic properties is a challenging task requiring complex experimental techniques. So far, a successful observation of magnetic domains in SRO thin films was demonstrated by means of Lorentz transmission electron microscopy [16]. This technique, however, puts additional requirements for sample preparation, which leads to further difficulties during the measurement process itself, making the whole experimental procedure more complex and difficult. On the other hand, the low temperature MFM is powerful enough to provide access to information about magnetic properties while putting none additional requirements on sample preparation, making the experimental procedure easily feasible. There has already been one MFM study observing magnetic domains in SRO [28], however, the SRO was in a form of patterned nanoislands, and therefore exhibiting different magnetization dynamics compared to this study. Here the first MFM study of magnetization reversal in SRO thin films is presented, demonstrating the potential of this method in complex investigation of ferromagnetic materials with low Curie temperature.

## 2. Experimental details

Investigated SRO films were prepared by pulsed deposition on (001) oriented STO substrates with Ti termination. Growth of SRO on STO substrate is possible in six different crystallographic orientations, so called variants [15, 29]. Low miscut angle of the substrate leads to coexistence of several variants, i.e. to growth of polycrystalline films. Higher miscut angle leads to suppression of multi-variant growth [30, 15, 29], therefore we used substrates of 1° and 0.1° of miscut angles to achieve growth of single-variant (SRO1) and multi-variant (SRO2) films, respectively.

The pulsed laser deposition process was carried out under background oxygen pressure of 120 mTorr. A KrF laser at a wavelength of 248 nm was used, with typical growth rate of 15 pulses per monolayer and 2 Hz pulse-repetition rate. The STO substrate was kept at 900 K during the deposition process. Such parameters lead to single or poly-crystalline growth of SRO, depending on miscut angle of the STO substrate.

Proper crystallinity and surface morphology of the SRO films was verified by X ray diffraction (XRD) and atomic force microscopy (AFM), respectively. The XRD analysis was carried out using a PANanalytical X'Pert PRO diffractometer, measuring reciprocal space maps (RSM) around (204) family of STO Bragg reflections. SRO1 was found to be nearly single-variant, while presence of two crystallographic twins was revealed in SRO2. Thicknesses of the films were determined by the same instrument, symmetric scans around (002) Bragg reflection of SRO fitted by classical interference formula gave values of 28 nm (SRO1) and 46 nm (SRO2), respectively. The AFM images were taken at room temperature by a Bruker Dimension Edge AFM microscope.

The magnetization process was measured by SQUID magnetometer (Quantum design, MPMS7 XL, RSO option). To observe the change of magnetic domains in SRO thin films, low temperature atomic force microscope attoAFM/MFM Ixs was used, inserted in PPMS 14 (cryostat). The PPMS 14 does not allow a real zero-field cooling due to residual field of the superconducting coil, so the focus was made only on the magnetization process from fully magnetized state. The samples were magnetized at magnetic field of +3 T or higher (a control MFM scan was performed back at zero field for each sample). After that two measurement modes were chosen: (i) small negative field was applied and kept during the MFM measurement, (ii) small negative field was applied, and the MFM measurement was then performed at zero field to avoid further magnetization reversal process. MFM data were analyzed and plotted using Gwyddion software [31].

## 3. Results and discussion

### 3.1. Crystallographic properties and morphology

In order to determine crystallinity of the samples, RSM were measured for both SRO1 and SRO2. The results are shown in Figs. 1(a) and (b), respectively. The measurements were carried out at two azimuths for each sample. The out-of-plane component of reciprocal lattice vector  $Q_{\perp}$  is given as the out-of-plane projection of  $|Q| = 2 \sin(\theta) / \lambda$ , where  $\theta$  is the Bragg diffraction angle and  $\lambda = 1.5406 \text{ \AA}$ .

Fig. 1(a) shows the RSM of SRO on vicinal STO substrate (high miscut angle). The same lateral position of both STO and SRO peaks indicates that the film remains fully strained. Although a growth of only one crystallographic variant was expected on vicinal STO substrate, the RSM show presence of a second SRO variant as well. Above the main SRO peak a blurred side peak is visible. From intensity maxima the ratio of SRO peaks was roughly estimated as 1:9, which shows that the fraction of second crystallographic variant is very low, i.e. the SRO1 film is nearly single-variant.

Fig. 1(b) shows the RSM of SRO2. They reveal fully strained SRO even at higher thickness of the deposited layer. A growth of the second crystallographic variant was expected, and indeed the SRO side peaks are clearly visible. The volume of the second variant is significantly higher compared to SRO1. For SRO2 the ratio of SRO peaks was estimated

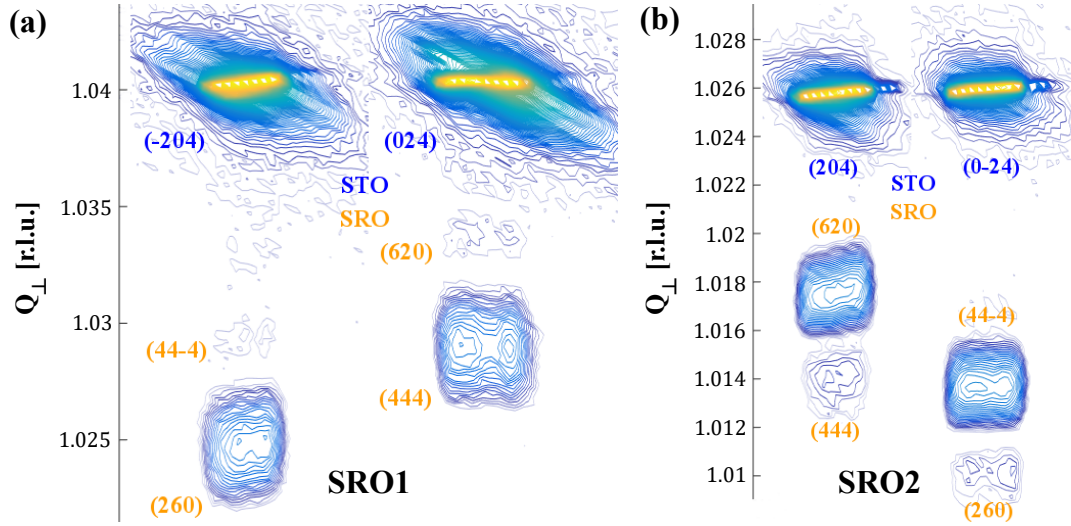


**Figure 1:** Reciprocal space maps around (204) family of Bragg reflections of SrTiO<sub>3</sub> measured on SrRuO<sub>3</sub> thin films deposited on (a) vicinal SrTiO<sub>3</sub> substrate (SRO1), ratio of the SrRuO<sub>3</sub> peaks was estimated as 1:9, i.e. the film is nearly single-variant; (b) SrTiO<sub>3</sub> substrate of low miscut angle (SRO2). Presence of two crystallographic SrRuO<sub>3</sub> twins is clearly visible, their ratio was estimated to be approximately 1:2.

to approximately 1:2. This means that the second crystallographic variant represents around 30% in case of SRO2, while it represents only 10% in case of SRO1.

A brief note should be made at this point, emphasizing that the thickness variation between the two films is not a leading cause of appearance of the second crystallographic variant. As already demonstrated by several research groups, the key factors in determining the crystallinity of SRO are the miscut angle and step direction of the STO substrate [15, 29, 30, 32]. Multiple variants could appear due to partial relaxation at higher thicknesses of the SRO layer, however, as demonstrated in Fig. 1, both investigated films are fully strained, leaving the substrate miscut angle as driving parameter for the observed differences in crystallinity.

Both samples, the nearly single-variant SRO1 and the multi-variant SRO2 were characterized by room temperature AFM as presented in Figs. 2(a) and (b), respectively. In both samples, atomic steps are clearly visible, which is a signature of good epitaxial growth of the films. Difference in the step width corresponds well to the different miscut angle of the substrates. In addition to atomic steps, Fig. 2(b) shows several island-like feature, which are a clear indication of 3D growth at higher thicknesses of deposited SRO layer. Higher surface roughness of SRO2 (1.6 nm) compared to SRO1 (0.3 nm) is due to high miscut angle of the vicinal substrate and step bunching during SRO growth [33].

### 3.2. Magnetic properties

The magnetization process was firstly studied by magnetometry measurements. In Fig. 3(a), magnetization loops of SRO1 and SRO2 samples are presented, measured at  $T = 20$  K with external magnetic field applied perpendicular to the sample surface. The field was ramped at 68 and 258  $\mu\text{T/s}$ , respectively. At these fast rates the coercive fields  $\mu_0 H_{C1,fast} = 145$  mT and  $\mu_0 H_{C2,fast} = 185$  mT were de-

termined. The measurement temperature of 20 K was chosen as optimal value with respect to Curie temperature ( $T_{C, film} \sim 150$  [12]) as well as with respect to the temperature-dependence curve of the SRO magnetic moment [11].

Magnetic moment of SRO in saturation at low temperature is  $1.6 \mu_B/\text{Ru}$  [34]. Saturation magnetization determined from Fig. 3(a) reaches  $1.5 \mu_B/\text{Ru}$  for SRO1, demonstrating high quality of the deposited SRO layer. The value determined for SRO2 is  $1.2 \mu_B/\text{Ru}$ , which is slightly lower compared to SRO1. This might be due to the presence of two SRO variants, and therefore lower crystalline quality of the sample. Presence of multiple crystallographic variants leads to intermediate areas among them, where the crystalline structure is not exactly defined. However, we assume that the effect would be very small as no significant additional broadening is visible in the XRD measurements. Unfortunately we are not aware of any previous research investigating this topic more in detail. Another possible explanation is discussed later in the section of Magnetic domains imaging.

Looking at the shape of the loops presented in Fig. 3(a), one can see that both loops exhibit square-like behaviour typical for loops measured along an easy axis of magnetization, which confirms that easy axis of both films has an out-of-plane component. One can also notice one particular difference in behaviour of these two loops. Around  $\pm 0.5$  T a small, but clearly remarkable drop of magnetization can be observed for SRO2. This shape of the hysteresis loop indicates two different contributions to the magnetic moment coming from the two different crystallographic variants. For SRO2 it is visible due to higher representation of the second SRO variant, while the magnetization drop becomes indistinct for SRO1. It confirms that the volume of the second variant is negligible, and that the SRO1 sample is nearly single-variant.

Fig. 3(b) shows the difference in the magnetization pro-

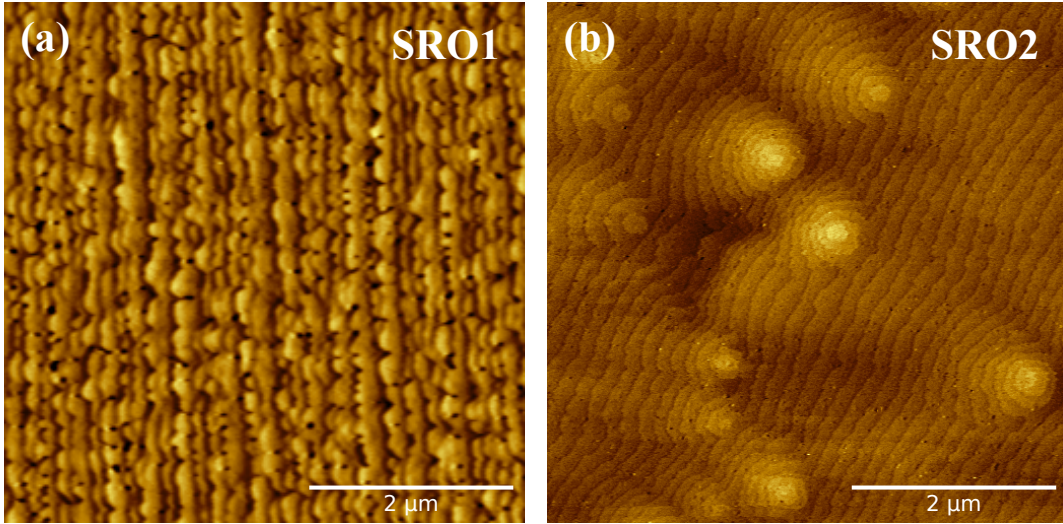


**Figure 2:** AFM images ( $5 \times 5 \mu\text{m}^2$ ) of (a) 28 nm thick nearly single-variant SrRuO<sub>3</sub> film (SRO1), surface roughness (RMS) is 1.6 nm; (b) 46 nm thick multi-variant SrRuO<sub>3</sub> film (SRO2), surface roughness (RMS) is 0.3 nm. Atomic steps are clearly visible for both films (vertical direction for SRO1, diagonal for SRO2), however the step bunching makes it a little less obvious for SRO1. For SRO2 three-dimensional islands can be seen as well.

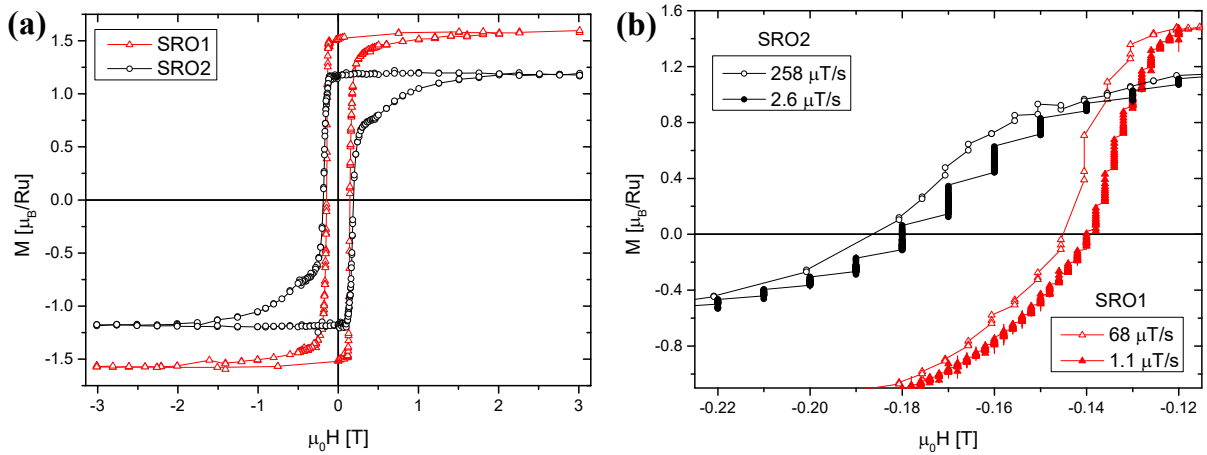


**Figure 3:** (a) Hysteresis loops of magnetization, (b) zoom of the hysteresis loops of magnetization near coercive field, measured at fast and slow rates. The data were recorded on nearly single-variant (SRO1) and multi-variant (SRO2) SrRuO<sub>3</sub> films by SQUID magnetometry at 20 K with magnetic field applied perpendicular to the sample surface. The pronounced field steps in (b) represent the actual field changes during the measurement. The slow ramping rates were realised by multiple data recording for a fixed period of time at a given value of the magnetic field, for which a gradual drop of magnetization can be observed at these values. See the text for more detailed explanation of the experimental procedure.

cess when ramping the magnetic field at different rate. For each sample there is a zoomed part of the loop presented in Fig. 3(a) compared to a loop measured at a slower rate, for SRO1 it is  $1.1 \mu\text{T/s}$ , for SRO2 it is  $2.6 \mu\text{T/s}$ . In case of the slow loops, lower values of the coercive field were found,  $\mu_0 H_{C1,slow} = 140 \text{ mT}$  and  $\mu_0 H_{C2,slow} = 180 \text{ mT}$  for SRO1 and SRO2, respectively. The difference represents 5 mT for both samples, clearly demonstrating a difference in the dynamics of the magnetization reversal process. For the slow field ramping in Fig. 3(b), multiple data points for each field value are visible. That is because in the vicinity of coercive field, the magnetic field was kept at a constant value for 27 (SRO1) and 60 (SRO2) min while measuring a

set of few hundred data points. Thus for each value of the magnetic field time evolution of magnetization is clearly visible. Lines in the figure are guides to the eye, connecting the data points in chronological order of recording. The average ramping rate is then calculated across the whole region around coercive field.

A note should be made here addressing the issue of slightly different thicknesses of the investigated films. One might express doubts, whether any differences observed in the magnetization behaviour could not be attributed to changes of this parameter. However, any thickness dependent changes in magnetization behaviour (such as  $T_C$  or magnetic anisotropy) are typically governed by interfacial effects, and therefore they

are taking place in the ultrathin region of thicknesses below  $\sim 9$  monolayers [2, 35, 36]. Thicknesses of the films presented here are well above this threshold for the so-called thick film behaviour, where no such effects were shown to take place. The only quantity that continues changing beyond this limit remains to be the saturation magnetization. However, data presented in Fig. 3 are corrected for these changes via normalisation to formula units, showing that the thicker film exhibits even lower saturation magnetization, which further supports variants-related phenomena as a key parameter in determining the magnetic properties. Magnetization changes could also take place due to strain relaxation of the films with increasing thickness, however as shown in Fig. 1, both films remained fully strained up to 46 nm of film thickness, which safely rules out any potential influence of thickness variation on magnetic properties of the SRO films.

### 3.3. Magnetic domains imaging

The magnetization process was visualised employing low temperature magnetic force microscopy. A typical series of MFM scans of SRO1, taken at 20 K, is shown in Fig. 4. Duration of each scan was approximately 45 min. The slow scan direction is indicated by a black arrow in the figure. The first scan (shown in Fig. 4(a)) was taken after saturating the sample at +3 T. One can see a homogeneously magnetized area of the sample with a signature of the atomic steps, coming from the crosstalk of topography (cf. Fig. 2(a)). Then a small negative field of -119 mT was applied and kept during the measurement. The beginning of magnetization reversal process is shown in Fig. 4(b). Bright areas represent the initial magnetization, while the dark areas are reversed. The homogeneous bottom half of the image is still fully saturated. After approximately 20 min, the large bright area abruptly ends as the first switching event is covered by the horizontal movement of the scanner. As expected from the SQUID magnetization measurements (cf. Fig. 3(b)), the magnetization reversal process further continues in time as shown in Fig. 4(c) taken right after the first scan while keeping the same field of -119 mT. Further increment of the reversed (dark) area can still be observed after nearly 4 h at the same magnetic field, as demonstrated in Fig. 4(d). Such slow time evolution of the magnetic domain pattern is in agreement with the magnetization relaxation observed by SQUID (cf. Fig. 3(b)). However, it is the contrary of an MFM study of magnetization reversal in patterned nanoislands of SRO, presented by Landau *et al.* [28]. They observed no relaxation effects in the SRO nanoislands. Such behaviour can be satisfactorily explained in terms of the strong shape anisotropy induced by patterning into the nanostructures. On the other hand, there is no such contribution to magnetic anisotropy in our films, therefore the relaxation effects remain observable.

Fig. 5 shows a series of MFM scans taken at 20 K on SRO2. Duration of each scan was approximately 13 min. Fig. 5(a) shows saturated state measured in remanence after application of +3 T. One can see a homogeneously magnetized area

with two kind of features. First, weak dark shadow spots, coming from the crosstalk of topography (cf. Fig. 2(b)), are visible all over the investigated area. Then, several bubble-like features with non-regular shape can be seen across the image. Two of them are indicated by white arrows. These features clearly exhibit magnetic signal that cannot be erased even in magnetic fields up to 14 T, which was the largest field in our experimental setup. The exact nature of the bubble-like features was not unambiguously clarified, but we assume that they can be related to crystallographic defects, such as anti-phase boundaries (APB) [37], arising in the multi-variant growth. Such defects may consequently lead to creation of small areas with antiferromagnetic ordering, whose magnetic signal can persist up to high magnetic fields, as reported for example in magnetite [38]. Then these crystallographic defects can also act as domain nucleation centers, which indeed was observed by means of MFM.

Fig. 5(b) shows the MFM scan taken after application of small negative field of -140 mT, where the two bubble-like features indicated by arrows in Fig. 5(a) become domain nucleation centers. The dark magnetic domains are clearly originating in these two persistent magnetic structures. The reversed area of the image increases in time as shown in Fig. 5(c), taken after 52 min from the initial field application. As demonstrated in Fig. 5(d), the magnetization pattern still evolves after nearly two hours, exhibiting similar timescale of several hours as in case of the magnetization relaxation in SRO1 (cf. Fig. 4). The only apparent difference in the magnetization reversal process then remains in the size of the magnetic domains, which are markedly smaller in the SRO2 sample. Note that the scan size in Fig. 5 is larger compared to scans in Fig. 4, as we were trying to cover larger area when searching for the domain nucleation process. Yet the difference in the domain size is evident, suggesting that the density of pinning centers is higher in SRO2, which leads to more indented domain pattern.

A note should be made here that due to different densities of pinning centers the relaxation effects might be expected to occur on different timescales in both films. Although the magnetization relaxation was observed on comparable timescales of several hours, the relaxation behaviour was not investigated on longer timescale, where such possible differences might become noticeable.

The bubble-like features also lead to another important observation. As their magnetic signal is persistent up to high magnetic fields ( $\sim 14$  T), in the hysteresis loop of SRO2 measured up to 3 T (see Fig. 3(a)) there is no observable change of the magnetization slope associated with these features. However their mere presence automatically leads to decrease of the saturated area of the sample, which should manifest itself via decrease of the overall saturation magnetization. That is exactly the result presented in Fig. 3(a). Therefore one can conclude that the observed saturation magnetization decrease is also related to crystallographic defects, such as APB, which arise in the multi-variant growth, and whose persistent magnetic signal prevents the SRO film from its full saturation.

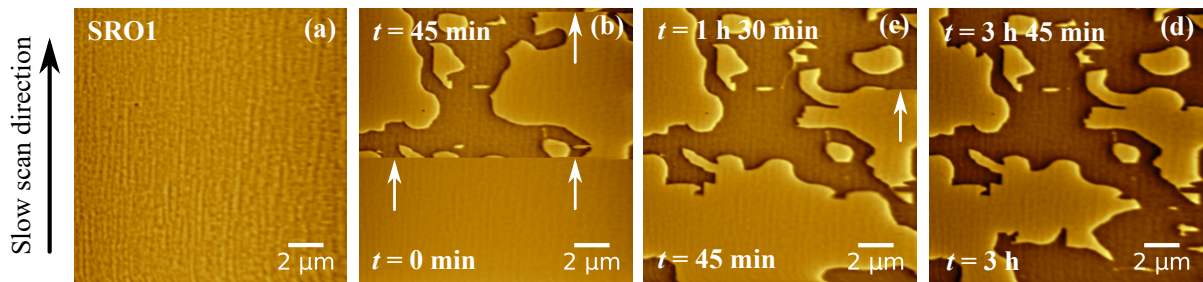


**Figure 4:** MFM images ( $15 \times 15 \mu\text{m}^2$ ) of magnetization reversal in nearly single-variant SrRuO<sub>3</sub> film (SRO1) measured at 20 K with field applied perpendicular to the sample surface. Slow scan direction was vertical, proceeding upwards, as indicated by the black arrow. (a) Fully saturated state measured at +3 T, (b) first scan at -119 mT, where beginning of the switching process can be seen, (c) second scan at -119 mT measured right after the first scan, (d) last scan at -119 mT after nearly 4 h, further magnetization evolution is still visible. White arrows in (b) and (c) point out horizontal division lines between bright (initial) and dark (reversed) areas that are just being switched during the scan. Areas below these lines appear switched in following image. The time after field application is indicated for the beginning (bottom) and the end (top) of each scan.

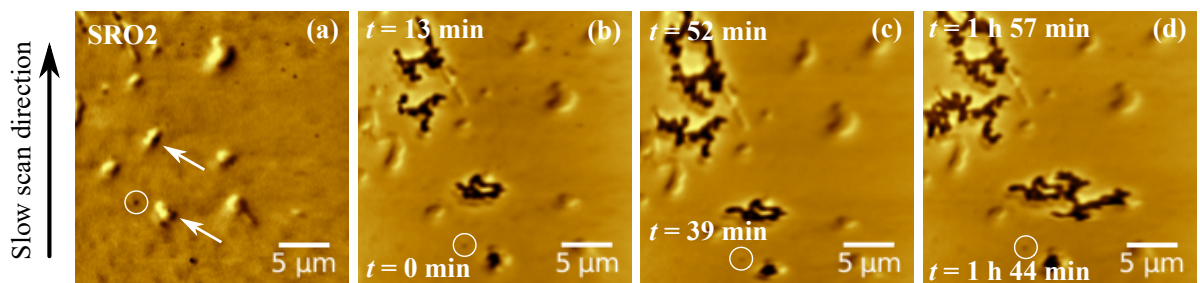


**Figure 5:** MFM images ( $26 \times 26 \mu\text{m}^2$ ) of magnetization reversal in multi-variant SrRuO<sub>3</sub> film (SRO2) measured at 20 K with field applied perpendicular to the sample surface. Slow scan direction is indicated by the black arrow. Bright areas represent initial magnetization, dark areas are reversed. (a) Fully magnetized state, measured in remanence after saturation in +3 T, (b) first scan at -140 mT where domain nucleation is captured, (c) one of the following scans at -140 mT measured after 52 min, (d) last scan at -140 mT after nearly 2 h. White circle in all images highlights a dirt particle that serves as a marker. White arrows in (a) indicate bubble-like features acting as domain nucleation centers. The time after field application is indicated for the beginning (bottom) and the end (top) of each scan.

Fig. 6(a) shows a single scan of SRO2 taken at a higher negative field of -180 mT. The scan was measured right after the field application, but here the aim is not to discuss the dynamics. We want to point out that more than a half of the area is already reversed, which means that the overall magnetic moment of the sample should be negative. However this scan was taken at a field value determined as coercive field  $\mu_0 H_{C2,slow}$  according to the SQUID magnetometry (see Fig. 3(b)). This disagreement between MFM and SQUID points out the local character of the MFM measurement, as only a small area of the sample can be measured during the scan. Nevertheless, despite the quantitative inaccuracy of the MFM, conclusions on behaviour of magnetic domains remain unequivocal.

As demonstrated in Fig. 5, in SRO2 sample we were able to observe the domain nucleation process, which enabled determination of the nucleation centers. On the other hand this was not possible on SRO1, where we did not succeed in capturing the exact location of the nucleation centers. As already presented earlier, in Fig. 4(b) the very beginning of the switching process was captured, and yet a clearly demarcated area indicating a nucleation center is not visible. The reversed (dark) area is missing borders on the left and

top edge of the image, suggesting that the domain nucleated outside the observed area. In order to locate the domain nucleation centers, we tried to find one clearly demarcated reversed domain by observing a larger area of the sample. First a single MFM scan was measured, at a small negative field of -117 mT where a switching event appeared. Then the magnetic field was turned off to prevent further propagation of magnetic domains, and the scanner was moved around the area of the sample to find borders of the initially observed reversed domain. This way an area of  $90 \times 90$  squared micrometers was investigated, as shown in Fig. 6(b). However, we were not able to find borders of the reversed region, i.e. we did not locate the domain nucleation centers.

A remark should be made here, mentioning that one can also suggest an alternative explanation for the process depicted in Fig. 4. If one assumes that the domain nucleated in the very center of Fig. 4(b), and that the reversal process then occurred very quickly, it would be possible that the domain walls propagated from the center beyond the image borders before the scan was finished. In order to test this hypothesis, several control measurements were performed in a following sequence. Firstly, the sample was saturated in a high positive field, and a small negative field (e.g. -120 mT) was



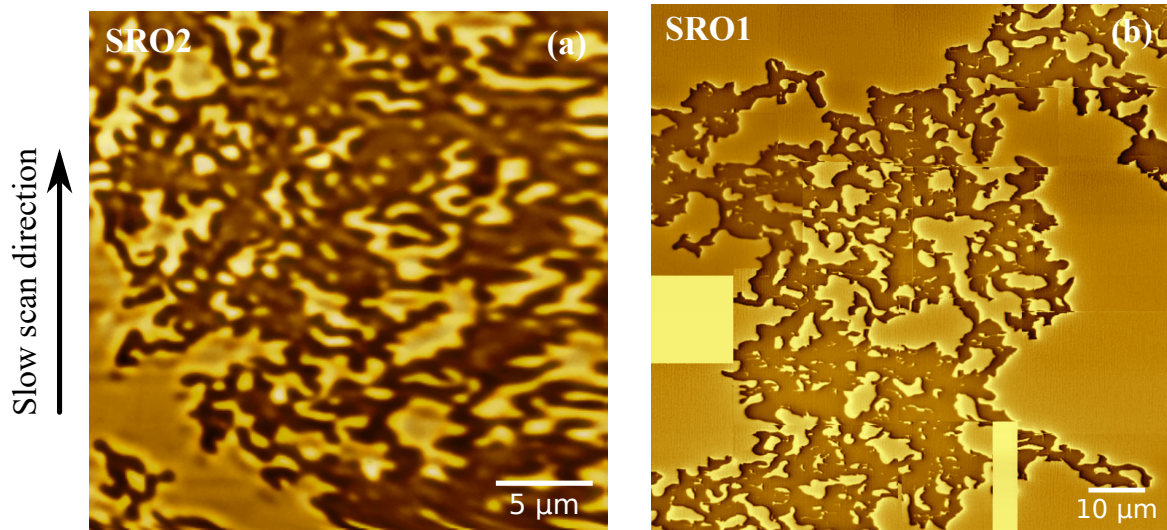


**Figure 6:** MFM images: (a)  $26 \times 26 \mu\text{m}^2$  area of multi-variant SrRuO<sub>3</sub> film, measured at 20 K with field of -180 mT applied perpendicular to the sample surface. (b)  $90 \times 90 \mu\text{m}^2$  area in single-variant SrRuO<sub>3</sub> film (SRO1) composed of several  $26 \times 26 \mu\text{m}^2$  scans taken at 20 K, at remanence after initiation of the switching process with field of -117 mT perpendicular to the sample surface. Slow scan direction is indicated by the black arrow.

applied to initiate the nucleation process, after which a first image was captured. Secondly, the sample was saturated in a high positive field again, and then a small negative field was applied, of lower amplitude compared to the first measurements (e.g. -115 mT). Now a second image was captured and the domain pattern was compared with the first image. As the second image was recorded at lower field, the reversed area should be smaller compared to the first image, allowing to determine the direction of domain wall propagation, as well as the relative position of the nucleation center. If the nucleation center were located in the middle of the observed area, the domain walls would propagate from the middle, and the reversed area would be diminished at the borders. However, the measurements revealed the exact opposite, i.e. the reversed area was significantly diminished in the middle, suggesting that the domain wall propagation was proceeding from outside into the investigated area. This leaves the alternative hypothesis highly unlikely. The domain nucleation center always appeared to be located outside the observed area. Together with the findings from Fig. 6(b), it leaves us unable to determine the exact position of domain nucleation centers.

Not being able to capture the domain nucleation in SRO1 indicates significantly lower density of the nucleation centers in SRO prepared on vicinal STO substrate. Properties of the magnetic domains are also different between the two films. SRO1 exhibits larger magnetic domains and smaller coercive field, which both indicate lower density of pinning centers in SRO on vicinal substrate. The low density of both the pinning and the nucleation centers is likely to be related to density of crystallographic defects. Presence of the defects is apparently suppressed in SRO on vicinal substrate via suppression of the multi-variant growth. Even though the growth of purely single-variant SRO film was not achieved,

the representation of second crystallographic variant in case of SRO1 is so low that the magnetic properties are notably improved. Absence of the bubble-like features in MFM measurements on SRO1 further support their relation to crystallographic defects, such as APB, which were reported as typical defects in SRO thin films [15, 39, 40]. APB can lead to antiferromagnetic ordering inducing magnetic signal that can persist up to high magnetic fields [38]. Even though there are no MFM reports on similar behaviour in SRO films, a recent study reported almost identical MFM features arising near APB in bulk Ni-Mn-Ga [41]. It can therefore be inferred that growth of SRO on vicinal STO substrate leads to reduced density of crystallographic defects acting as domain nucleation centers, such as APB, and consequently to significantly improved magnetic properties of the films.

#### 4. Conclusions

A study of the influence of substrate miscut on magnetic properties of SRO ultrathin films was performed. As expected, the structural investigation showed that multi-variant growth can be successfully suppressed by use of vicinal (high miscut angle) STO substrate. By means of SQUID magnetometry and MFM microscopy the magnetization dynamics and behaviour of the magnetic domains was studied. Magnetization relaxation was found to take place in both the multi-variant and the nearly single-variant SRO films. The relaxation effects were observed on similar timescale of several hours in both films. It was further found that the multi-variant film exhibits higher coercive field and smaller magnetic domains, which is directly related to higher density of pinning centers, i.e. higher density of crystallographic defects. High density of defects was confirmed also by direct observation of the domain nucleation centers, which are likely to originate due to the enhanced multi-variant growth.

We believe that some of the defects are anti-phase boundaries, leading to antiferromagnetic ordering and persistent features in MFM signal up to high magnetic fields. Presence of such unsaturated magnetic structures results in lower saturation magnetization of the multi-variant film. Growth of SRO on vicinal STO substrate therefore leads to reduced density of crystallographic defects, i.e. to better overall crystalline quality of the films, and consequently to improved magnetic properties of SRO. Such results are of high importance for design and further applications in oxide spintronics and electronics, because it will allow direct tuning of magnetic properties via substrate miscut angle or other deposition parameters.

## Acknowledgments

The SQUID magnetometry and MFM microscopy experiments were performed in MGML ([www.mgml.eu](http://www.mgml.eu)), which is supported within the program of Czech Research Infrastructures, Project No. LM2018096. The research was further supported by the Ministry of Education, Youth and Sports of Czech Republic by OP VVV, Project MATFUN No. CZ.02.1.01/0.0/0.0/15\_003/0000487. This work was also supported by GAČR, Project No. 19-09882S. This work was further supported by a PHC Barrande grant of the French Ministry for Europe and Foreign Affairs, Project No. 34000QK.

## Data availability

The raw data required to reproduce these findings cannot be shared at this time as the data also forms part of an ongoing study. The processed data required to reproduce these findings cannot be shared at this time as the data also forms part of an ongoing study.

## CRedit authorship contribution statement

**Martin Zahradník:** Investigation, Formal Analysis, Visualization, Data Curation, Writing - Original Draft. **Klára Uhlířová:** Conceptualization, Methodology, Investigation, Validation, Project Administration, Writing - Review & Editing. **Thomas Maroutian:** Resources, Methodology, Conceptualization, Investigation, Writing - Review & Editing. **Georg Kurij:** Investigation. **Guillaume Agnus:** Supervision. **Martin Veis:** Conceptualization, Funding Acquisition, Writing - Review & Editing, Supervision. **Philippe Lecoeur:** Funding Acquisition, Supervision.

## References

- [1] A. Kanbayasi, Magnetic properties of srruo3 single crystal, *Journal of the Physical Society of Japan* 41 (1976) 1876–1878.
- [2] G. Koster, L. Klein, W. Siemons, G. Rijnders, J. S. Dodge, C.-B. Eom, D. H. A. Blank, M. R. Beasley, Structure, physical properties, and applications of srruo<sub>3</sub> thin films, *Rev. Mod. Phys.* 84 (2012) 253–298.
- [3] B. Allouche, Y. Gagou, F. L. Marrec, M.-A. Fremy, M. E. Marssi, Bipolar resistive switching and substrate effect in gdk2nb5o15 epitaxial thin films with tetragonal tungsten bronze type structure, *Materials & Design* 112 (2016) 80–87.
- [4] G. Herranz, B. Martínez, J. Fontcuberta, F. Sánchez, M. V. García-Cuenca, C. Ferrater, M. Varela, SrRuO<sub>3</sub>/SrTiO<sub>3</sub>/SrRuO<sub>3</sub> heterostructures for magnetic tunnel junctions, *Journal of Applied Physics* 93 (2003) 8035–8037.
- [5] D. C. Worledge, T. H. Geballe, Negative spin-polarization of srruo<sub>3</sub>, *Phys. Rev. Lett.* 85 (2000) 5182–5185.
- [6] K. S. Takahashi, A. Sawa, Y. Ishii, H. Akoh, M. Kawasaki, Y. Tokura, Inverse tunnel magnetoresistance in all-perovskite junctions of la<sub>0.7</sub>sr<sub>0.3</sub>mno<sub>3</sub>/srtio<sub>3</sub>/srruo<sub>3</sub>, *Phys. Rev. B* 67 (2003) 094413.
- [7] X. Ke, M. S. Rzchowski, L. J. Belenky, C. B. Eom, Positive exchange bias in ferromagnetic la<sub>0.67</sub>sr<sub>0.33</sub>mno<sub>3</sub>?srruo<sub>3</sub> bilayers, *Applied Physics Letters* 84 (2004) 5458–5460.
- [8] X. Ke, L. J. Belenky, C. B. Eom, M. S. Rzchowski, Antiferromagnetic exchange-bias in epitaxial ferromagnetic la<sub>0.67</sub>sr<sub>0.33</sub>mno<sub>3</sub>?srruo<sub>3</sub> bilayers, *Journal of Applied Physics* 97 (2005) 10K115.
- [9] P. Padhan, W. Prellier, R. C. Budhani, Antiferromagnetic coupling and enhanced magnetization in all-ferromagnetic superlattices, *Applied Physics Letters* 88 (2006) 192509.
- [10] A. Solignac, R. Guerrero, P. Gogol, T. Maroutian, F. Ott, L. Largeau, P. Lecoeur, M. Pannetier-Lecoeur, Dual antiferromagnetic coupling at la<sub>0.67</sub>sr<sub>0.33</sub>mno<sub>3</sub>/srruo<sub>3</sub> interfaces, *Phys. Rev. Lett.* 109 (2012) 027201.
- [11] G. Kurij, Magnetic tunnel junctions for ultrasensitive all-oxide hybrid sensors for medical applications, Ph.D. thesis, Université Paris-Saclay, 2016. URL: <https://tel.archives-ouvertes.fr/tel-01359180>.
- [12] C. B. Eom, R. J. Cava, R. M. Fleming, J. M. Phillips, R. B. vanDover, J. H. Marshall, J. W. P. Hsu, J. J. Krajewski, W. F. Peck, Single-crystal epitaxial thin films of the isotropic metallic oxides sr1-xcaxruo<sub>3</sub> (0 ≤ x ≤ 1), *Science* 258 (1992) 1766–1769.
- [13] Y. Kats, I. Genish, L. Klein, J. W. Reiner, M. R. Beasley, Large anisotropy in the paramagnetic susceptibility of SrRuO<sub>3</sub> films, *Phys. Rev. B* 71 (2005) 100403.
- [14] L. Klein, J. S. Dodge, C. H. Ahn, J. W. Reiner, L. Mieville, T. H. Geballe, M. R. Beasley, A. Kapitulnik, Transport and magnetization in the badly metallic itinerant ferromagnet srruo<sub>3</sub>, *Journal of Physics: Condensed Matter* 8 (1996) 10111.
- [15] J. C. Jiang, W. Tian, X. Q. Pan, Q. Gan, C. B. Eom, Domain structure of epitaxial srruo<sub>3</sub> thin films on miscut (001) srtio<sub>3</sub> substrates, *Applied Physics Letters* 72 (1998) 2963–2965.
- [16] A. F. Marshall, L. Klein, J. S. Dodge, C. H. Ahn, J. W. Reiner, L. Mieville, L. Antagonazza, A. Kapitulnik, T. H. Geballe, M. R. Beasley, Lorentz transmission electron microscope study of ferromagnetic domain walls in srruo<sub>3</sub>: Statics, dynamics, and crystal structure correlation, *Journal of Applied Physics* 85 (1999) 4131–4140.
- [17] Q. Gan, R. A. Rao, C. B. Eom, L. Wu, F. Tsui, Lattice distortion and uniaxial magnetic anisotropy in single domain epitaxial (110) films of srruo<sub>3</sub>, *Journal of Applied Physics* 85 (1999) 5297–5299.
- [18] S. Kolesnik, Y. Z. Yoo, O. Chmaissem, B. Dabrowski, T. Maxwell, C. W. Kimball, A. P. Genis, Effect of crystalline quality and substitution on magnetic anisotropy of srruo<sub>3</sub> thin films, *Journal of Applied Physics* 99 (2006) 08F501.
- [19] M. Feigenson, J. W. Reiner, L. Klein, Current-induced magnetic instability in srruo<sub>3</sub>, *Journal of Applied Physics* 103 (2008) 07E741.
- [20] M. Feigenson, J. W. Reiner, L. Klein, Efficient current-induced domain-wall displacement in srruo<sub>3</sub>, *Phys. Rev. Lett.* 98 (2007) 247204.
- [21] B. Sarkar, B. Dalal, S. K. De, Temperature induced magnetization reversal in srruo<sub>3</sub>, *Applied Physics Letters* 103 (2013) 252403.
- [22] Y. Shperber, D. Bedau, J. W. Reiner, L. Klein, Current-induced magnetization reversal in srruo<sub>3</sub>, *Phys. Rev. B* 86 (2012) 085102.
- [23] Y. Shperber, O. Sinwani, N. Naftalis, D. Bedau, J. W. Reiner, L. Klein, Thermally assisted current-induced magnetization reversal in srruo<sub>3</sub>, *Phys. Rev. B* 87 (2013) 115118.
- [24] W. P. Zhou, Q. Li, Y. Q. Xiong, Q. M. Zhang, D. H. Wang, Q. Q. Cao, L. Y. Lv, Y. W. Du, Electric field manipulation of magnetic and transport properties in srruo<sub>3</sub>/pb(mg<sub>1/3</sub>nb<sub>2/3</sub>)o<sub>3</sub>-pbtio<sub>3</sub> heterostructure, *Scientific Reports* (2014).

- [25] H. Barkhausen, Zwei mit Hilfe der neuen Verstärker entdeckte Erscheinungen, *Phys. Z* 20 (1919) 401.
- [26] J. Pommier, P. Meyer, G. Pénissard, J. Ferré, P. Bruno, D. Renard, Magnetization reversal in ultrathin ferromagnetic films with perpendicular anisotropy: Domain observations, *Phys. Rev. Lett.* 65 (1990) 2054–2057.
- [27] A. Schwarz, M. Liebmann, U. Kaiser, R. Wiesendanger, T. W. Noh, D. W. Kim, Visualization of the Barkhausen effect by magnetic force microscopy, *Phys. Rev. Lett.* 92 (2004) 077206.
- [28] L. Landau, J. W. Reiner, L. Klein, Low temperature magnetic force microscope study of magnetization reversal in patterned nanoislands of SrRuO<sub>3</sub>, *Journal of Applied Physics* 111 (2012) 07B901.
- [29] J. Jiang, W. Tian, X. Pan, Q. Gan, C. Eom, Effects of miscut of the SrTiO<sub>3</sub> substrate on microstructures of the epitaxial SrRuO<sub>3</sub> thin films, *Materials Science and Engineering: B* 56 (1998) 152 – 157.
- [30] Q. Gan, R. A. Rao, C. B. Eom, Control of the growth and domain structure of epitaxial SrRuO<sub>3</sub> thin films by vicinal (001) SrTiO<sub>3</sub> substrates, *Applied Physics Letters* 70 (1997) 1962–1964.
- [31] D. Nečas, P. Klapetek, Gwyddion: an open-source software for SPM data analysis, *Central European Journal of Physics* 10 (2012) 181–188.
- [32] A. Vailionis, W. Siemons, G. Koster, Strain-induced single-domain growth of epitaxial SrRuO<sub>3</sub> layers on SrTiO<sub>3</sub>: A high-temperature x-ray diffraction study, *Applied Physics Letters* 91 (2007) 071907.
- [33] D. Estève, T. Maroutian, V. Pillard, P. Lecoeur, Step velocity tuning of SrRuO<sub>3</sub> step flow growth on SrTiO<sub>3</sub>, *Phys. Rev. B* 83 (2011) 193401.
- [34] S. Bushmeleva, V. Pomjakushin, E. Pomjakushina, D. Sheptyakov, A. Balagurov, Evidence for the band ferromagnetism in SrRuO<sub>3</sub> from neutron diffraction, *Journal of Magnetism and Magnetic Materials* 305 (2006) 491 – 496.
- [35] J. Xia, W. Siemons, G. Koster, M. R. Beasley, A. Kapitulnik, Critical thickness for itinerant ferromagnetism in ultrathin films of SrRuO<sub>3</sub>, *Phys. Rev. B* 79 (2009) 140407.
- [36] K. Ishigami, K. Yoshimatsu, D. Toyota, M. Takizawa, T. Yoshida, G. Shibata, T. Harano, Y. Takahashi, T. Kadono, V. K. Verma, V. R. Singh, Y. Takeda, T. Okane, Y. Saitoh, H. Yamagami, T. Koide, M. Oshima, H. Kumigashira, A. Fujimori, Thickness-dependent magnetic properties and strain-induced orbital magnetic moment in SrRuO<sub>3</sub> thin films, *Phys. Rev. B* 92 (2015) 064402.
- [37] H. Zijlstra, Coping with Brown's paradox: The pinning and nucleation of magnetic domain walls at antiphase boundaries, *IEEE Transactions on Magnetics* 15 (1979) 1246–1250.
- [38] D. T. Margulies, F. T. Parker, M. L. Rudee, F. E. Spada, J. N. Chapman, P. R. Aitchison, A. E. Berkowitz, Origin of the anomalous magnetic behavior in single crystal Fe<sub>3</sub>O<sub>4</sub> films, *Phys. Rev. Lett.* 79 (1997) 5162–5165.
- [39] N. D. Zakharov, K. M. Satyalakshmi, G. Koren, D. Hesse, Substrate temperature dependence of structure and resistivity of SrRuO<sub>3</sub> thin films grown by pulsed laser deposition on (100) SrTiO<sub>3</sub>, *Journal of Materials Research* 14 (1999) 4385–4394.
- [40] S. H. Oh, J. H. Suh, C. G. Park, Defects in strained epitaxial SrRuO<sub>3</sub> films on SrTiO<sub>3</sub> substrates, *MATERIALS TRANSACTIONS* 48 (2007) 2556–2562.
- [41] L. Straka, L. Fekete, O. Heczko, Antiphase boundaries in bulk Ni-Mn-Ga Heusler alloy observed by magnetic force microscopy, *Applied Physics Letters* 113 (2018) 172901.